COORDINATED AIRBORNE STUDIES IN THE TROPICS (CAST)

N. R. P. Harris, L. J. Carpenter, J. D. Lee, G. Vaughan, M. T. Filus, R. L. Jones, B. OuYang, J. A. Pyle, A. D. Robinson, S. J. Andrews, A. C. Lewis, J. Minaeian, A. Vaughan, J. R. Dorsey, M. W. Gallagher, M. Le Breton, R. Newton, C. J. Percival, H. M. A. Ricketts, S. J.-B. Bauguitte, G. J. Nott, A. Wellpott, M. J. Ashfold, J. Flemming, R. Butler, P. I. Palmer, P. H. Kaye, C. Stopford, C. Chemel, H. Boesch, N. Humpage, A. Vick, A. R. MacKenzie, R. Hyde, P. Angelov, E. Meneguz, and A. J. Manning

The CAST project involves studying the chemical composition of the atmosphere in the tropical warm pool region to improve our understanding of trace gas transport in convection.

The tropical tropopause layer (TTL) is the region of the tropical atmosphere between the main convective outflow at around 12–13 km and the base of the stratosphere at 17–18 km and is a very important region for composition–aerosol–climate interactions (Randel and Jensen 2013). Its overall structure is intermediate between the troposphere and stratosphere, with a lapse rate smaller than the saturated adiabatic up to the cold point (Fueglistaler et al. 2009). This is caused by the combined effect of slow radiative processes and the infrequent penetration of convective turrets to high altitudes. There is a marked longitudinal asymmetry in TTL temperatures, with a minimum in the region 130°E–180° during all times of the year. This minimum corresponds to the warm waters of the tropical warm pool (TWP) beneath, and there is an associated maximum in convection (Gettelman et al. 2002). The TTL is the predominant route for troposphere-to-stratosphere transport, so that conditions in the TTL set the entry concentrations at the base of the stratosphere for, for example, stratospheric water vapor and very short-lived halogen species. Knowledge of the input into the TTL is a prerequisite for correct modeling of TTL (and hence stratospheric) composition and yet many aspects are poorly constrained (Levine et al. 2007; Heyes et al. 2009). The couplings between the various processes are important. For example, improving the treatment of TTL water vapor and cirrus in global climate models requires a better understanding of convective transport and radiative transfer in the TTL, as well as improved model descriptions of the key processes.

We are still unclear about the entry and exit routes for the TTL, including how much material is transported quasi horizontally into the extratropical lowermost stratosphere (Levine et al. 2008). What is the average residence time in the TTL? What is the nature, and importance for composition, of longitudinal variability within the TTL? How much of the very short-lived halogen species can pass through the TTL and so affect stratospheric ozone concentrations? Large discrepancies exist between models and measurements even for long-lived tracers. Some of these are due to transport—sharp horizontal gradients are observed in atmospheric tracers at boundaries between midlatitude, subtropical, and tropical air masses, which are not well represented by models (Wofsy et al. 2011)—and some to limited information on emissions [e.g., N_2O and CH_4 in this region; Ishijima et al. (2010)]. These issues are more important for very short-lived substances (VSLSs, with lifetimes shorter than 6 months), including halogen-containing VSLSs with their poorly understood sources, atmospheric transformations, and geographic distributions (Carpenter et al. 2014). Other effects such as the degree to which the locations of the emissions coincide with strong convection can also have a strong influence on the overall flux (Russo et al. 2015).

To address these issues, the Facility for Airborne Atmospheric Measurements (FAAM) BAe-146 atmospheric research aircraft was deployed in Guam in January and February 2014 as part of the Coordinated Airborne Studies in the Tropics (CAST) campaign, a large multi-institutional project funded by the U.K. Natural Environment Research Council (NERC) and the Science and Technology Facilities Council (STFC). In Guam, it flew alongside the National Aeronautics and Space Administration's (NASA) Global Hawk, a high-altitude autonomous aircraft used in the NASA Airborne Tropical Tropopause Experiment (ATTREX) project, and the National Science Foundation/National Center for Atmospheric Research (NSF/NCAR) Gulfstream V (GV) in the NSF Convective Transport of Active Species in the Tropics (CONTRAST) project, as described in the companion papers by Jensen et al. (2017) and Pan et al. (2017). The measurements from all three campaigns are being jointly used to diagnose how air is carried high into the atmosphere.

The value inherent in having the three aircraft flying together was found in the ability to measure from the surface up into the stratosphere (see Fig. 1 in Pan et al. 2017). The instrument payloads on the three aircraft made many common measurements, which together have combined to provide a comprehensive dataset for interpretative studies. However, within this larger picture, each aircraft had its own scientific aims and objectives, which were appropriate to the specific aircraft's capabilities. The Global Hawk made measurements in the upper TTL (14–20 km), including in the outflow of convection. The GV aircraft principally sampled at the same altitudes as the main convective outflow (9–15 km) and, additionally, made measurements on profiles down into the boundary layer. In the case of the FAAM aircraft, the aims were to a) investigate halocarbon production in the marine boundary layer and b) characterize the composition of air in the main convective inflow. Knowledge of the distributions of trace gases in the boundary layer and lower troposphere is needed to estimate the flux of these gases into the TTL. The role of the FAAM research aircraft was to fly over the tropical west Pacific and to measure the composition in the lower troposphere (0–8 km). These measurements characterize the air masses in the region of the main convective inflow and so are valuable in interpreting the higher-altitude measurements of the Global Hawk and the GV made during the same period. They can also be used to improve our understanding of marine halocarbon production and to investigate the influence of polluted outflow from

AFFILIATIONS: Harris,* Filus, Jones, OuYang, and Robinson—Department of Chemistry, University of Cambridge, Cambridge, United Kingdom; Carpenter, Andrews, Minaeian, and A. Vaughan—Department of Chemistry, Wolfson Atmospheric Chemistry Laboratories, University of York, York, United Kingdom; Lee, G. Vaughan, and Ricketts—National Centre for Atmospheric Science, York, United Kingdom; Pyle—Department of Chemistry, University of Cambridge, and National Centre for Atmospheric Science, Cambridge, United Kingdom; Lewis—Department of Chemistry, Wolfson Atmospheric Chemistry Laboratories, University of York, York, United Kingdom, and National Centre for Atmospheric Science, York, United Kingdom; Dorsey—National Centre for Atmospheric Science, and School of Earth, Atmospheric and Environmental Science, University of Manchester, Manchester, United Kingdom; Gallagher, Le Breton, Newton, and Percival—School of Earth, Atmospheric and Environmental Science, University of Manchester, Manchester, United Kingdom; Bauguitte, Nott, and Wellpott—Facility for Airborne Atmospheric Measurements, Cranfield, United Kingdom; Ashfold—School of Biosciences, Malaysia Campus, University of Nottingham, Semenyih, Malaysia; Flemming—European Centre for Medium-Range Weather Forecasts, Reading, United Kingdom; Butler and Palmer—School of GeoSciences, University of Edinburgh, Edinburgh, United Kingdom; Kaye and Stopford—Centre for Atmospheric and Instrumentation Research, University of Hertfordshire, Hatfield, United Kingdom; Chemel—Centre for Atmospheric and Instrumentation Research, University of Hertfordshire, and National Centre for Atmospheric Science, University of Hertfordshire, Hatfield, United Kingdom; Boesch—Earth Observation Science, Department of Physics and Astronomy, and National Centre for Earth Observation, University of Leicester, United Kingdom; Humpage—Earth Observation Science, Department of Physics and Astronomy, University of Leicester, United Kingdom; Vick—U.K. Astronomy Technology Centre, Edinburgh, United Kingdom; MacKenzie—Birmingham Institute of Forest Research, University of Birmingham, Birmingham, United Kingdom; Hyde and Angelov—Data Science Group, Lancaster University, Lancaster, United Kingdom; Meneguz and Manning—Met Office, Exeter, United Kingdom

***CURRENT AFFILIATION:** Centre for Atmospheric Informatics and Emissions Technology, Cranfield University, Cranfield, United Kingdom

CORRESPONDING AUTHOR E-MAIL: Neil Harris, neil.harris@cranfield.ac.uk

The abstract for this article can be found in this issue, following the table of contents.

DOI:10.1175/BAMS-D-14-00290.1

In final form 2 February 2016

Asia. Additional measurements were made on Manus, Papua New Guinea.

The majority of this paper describes the CAST measurements during January–February 2014, as well as the flight planning tools used for the FAAM aircraft and for linking its measurements with those made by the other aircraft. Some early results are also discussed. The second CAST goal is to develop the U.K. capability to use autonomous aircraft for atmospheric research. Here, in addition to learning about deploying the Global Hawk and using the data collected, CAST scientists have produced two new instruments for use on the Global Hawk, which flew over the east Pacific during February–March 2015. These are described in the final section.

CAST MEASUREMENTS. Measurements were made on two main platforms in the west Pacific. The FAAM BAe-146 research aircraft was based at the A. B. Won Pat International Airport, Guam (13.5°N, 144.8°E). The FAAM aircraft was collocated with the NCAR Gulfstream while the NASA Global Hawk was based at Andersen Air Force Base, approximately 30 km to the northeast. A suite of ground-based instrument systems was based at the Atmospheric Radiation Measurement (ARM) facility at Manus (2.1°S, 147.4°E), in order to characterize the tropospheric composition beyond the range of the FAAM aircraft.

Flight planning. The goal of the CAST FAAM flights was to characterize the inflow to convection in the lower troposphere in the west Pacific. To extend the range of the aircraft so that it could reach into the upwelling area near the equator, overnight stops were planned at the islands of Palau (Roman Tmetuchl International Airport, Babeldaob island, Republic of Palau; 7.4°N, 134.5°E) and Chuuk (Chuuk International Airport, Weno Island, Federated States of Micronesia; 7.5°N, 151.8°E). When conditions allowed, transects were made at 100 feet (30.5 m) [with occasional dips down to 50 ft (15.2 m)] over the open ocean to give the opportunity to sample air influenced by fresh ocean emissions. Stacked runs with horizontal legs at different altitudes were planned where possible to provide information about the vertical profile of the short-lived species in the lower troposphere. A large part of the flight planning for the FAAM research aircraft was to ensure good coverage of the lower troposphere within range from Guam.

Chemical forecast products were provided by the Monitoring Atmospheric Composition and Climate (MACC) project in support of all three field campaigns. MACC assimilates comprehensive

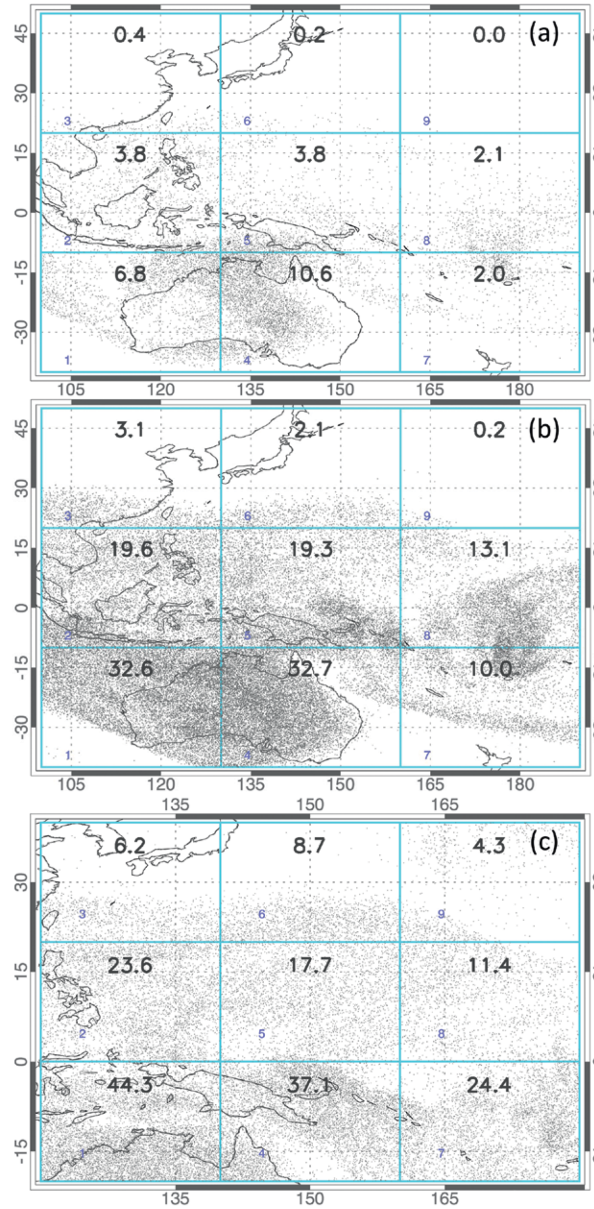

Fig. 1. Examples of trajectory-based forecast products used for multiaircraft flight planning. These plots are for 13 Feb 2014 when all three aircraft were in the same region [see Fig. 7 in Pan et al. (2016)]. The three panels show the location of air parcels which had been below 1-km altitude in the preceding 12 days at (a) 16–18, (b) 14–16, and (c) 12–14 km. The number in each box is the percentage of parcels in that box from below 1 km in the preceding 12 days. During the campaign, they were available as 1-, 3-, and 5-day forecasts for flight planning, and the NAME model was driven by analyses and forecasts from the Met Office operational model run at 25-km horizontal resolution.

global observations of chemical composition into the European Centre for Medium-Range Weather Forecasts (ECMWF) meteorological forecasting system (Flemming et al. 2015). The operational MACC

Table 1. Instruments and measurements made by the BAe-146 (FAAM) aircraft during the CAST project. Also indicated are the synergy with other aircraft from the CONTRAST (GV) and ATTREX (Global Hawk) projects.

Species/parameter	Method/instrument details	Averaging time	Precision, accuracy	Synergy with other aircraft	Affiliation; reference
Position, winds, u, v, w	Inertial navigation and global positioning system, five-port turbulence probe	0.1 s	$0.01\Delta P/P_s$	GV, GH	FAAM; Petersen and Renfrew (2009)
Humidity (dewpoint temperature)	Hygrometer, General Eastern 1011b	0.25 s	±0.5–±3 K, dependent on dewpoint and ambient conditions	GV, GH	FAAM; Ström et al. (1994)
Temperature	Rosemount Aerospace Ltd. sensor 102 AL	0.05 s	±0.3 K	GV, GH	FAAM; Lenschow (1986)
CO	Violet–ultraviolet (VUV) resonance/fluorescence, Aero Laser 5002	1 s	1 ppb, 3%	GV, GH	FAAM; Gerbig et al. (1999)
O_3	UV absorption, Thermo Environmental Instruments (TEI) model 49C	4 s	1 ppb, ±5%	GV, GH	FAAM; Wilson and Birks (2006)
CO_2, CH_4	Cavity Enhanced Absorption Spectrometer (CEAS), Los Gatos Research Inc.	1 s	CH_4: 2.5 ppb, 1.3 ppm; CO_2: 0.7 ppm, 0.2 ppm	GV, GH	FAAM, University of Manchester; O'Shea et al. (2013)
NO, NO_2	Chemiluminescence with photolytic conversion for NO_2, Air Quality Design Inc.	10 s	5 pptv for NO and 15 pptv for NO_2 (at 10-s averaging)	GV	FAAM–University of York; Lee et al. (2009)
Halocarbons (whole air samples): (DMS, $CHBr_3$, CH_2Br_2, $CHBr_2Cl$, CH_3I, CH_2BrCl, $CHBrCl_2$, CH_2ICl, CH_2IBr, CH_2I_2, CH_2Cl_2, $CHCl_3$)	TD-GC-MS, Markes	30-s fill time for WAS	Species dependent, typically 0.1–1 pptv	GV, GH	University of York; Andrews et al. (2013, 2016)
NMHCs (whole air samples): (C1–C7 NMHCs (alkanes, alkenes, aromatics); small o-VOCs (acetone, methanol, acetaldehyde, ethanol); DMS	GC-flame ionization detector (FID), Perkin Elmer	30-s fill time for WAS	Species dependent, typically 5 pptv	GV, GH	University of York; Hopkins et al. (2003)
Halocarbons, VOCs (in situ)	GC-MS, Agilent	300 s	Species dependent, typically 1–5 pptv	GV	University of York

Table 1. Continued.

Species/parameter	Method/instrument details	Averaging time	Precision, accuracy	Synergy with other aircraft	Affiliation; reference
BrO, Br_2, HOBr, BrCl, HCOOH (formic acid), HCN, $ClNO_2$, HNO_3, N_2O_5, CH_3COOH (acetic acid), CH_3CH_2COOH (propanoic acid), $CH_3CH_2CH_2COOH$ (butanoic acid)	CIMS	30 s	Species dependent, typically 0.3–5 ppt	GV	University of Manchester; Le Breton et al. (2012)
IO	Broadband (BB) CEAS	See text	See text	GV (IO remote sensing)	University of Cambridge; Kennedy et al. (2011)
PAN	Dual-column GC-ECD	90 s	3%, 10%	GV	University of York; Whalley et al. (2004)
Black carbon	Soot particle photometer (SP-2)	10 s	—	None	University of Manchester; Liu et al. (2015)
Aerosol	PCASP	1 s	See text	GV, GH	FAAM; Rosenberg et al. (2012)
Cloud physics	CDP	1 s	See text	GV, GH	FAAM; Rosenberg et al. (2012)

system runs at 80-km horizontal resolution (T255) with 60 vertical levels. During the campaign, forecast plots for the operation domain were provided for a number of chemical species, including the FAAM measurements: O_3, CO, CH_4, black carbon, NO, and NO_2. In addition, a number of hypothetical tracers were included to track air originating from different locations (e.g., regional emissions from China and India). A coastal emission tracer was used to track oceanic emissions of $CHBr_3$ and other short-lived halocarbons since these are preferentially released in coastal regions (Carpenter et al. 2009; Ashfold et al. 2014).

Linking measurements. To have near-real-time information about the air reaching the TTL from the lower troposphere, the trajectory-based approach of Ashfold et al. (2012) was adapted to meet the needs of a multiaircraft campaign. In this, the Numerical Atmospheric-Dispersion Modeling Environment (NAME) was run as an adjunct to the Met Office operational forecasting model so that it could access meteorological forecasts on a time scale quick enough to provide useful flight-planning information. The starting grid for the trajectories covered a large area of the west Pacific (Fig. 7), with trajectories being released at altitudes between 8 and 18 km. Twelve-day backward trajectories were then calculated using a mixture of Met Office analyses and forecasts, so that information was available about the possible influence of lower-tropospheric air in the regions that could be sampled by the Global Hawk and the GV. Each day, trajectories were produced for 1, 2, 3 and 5 days into the future. In each 2-km-altitude layer, 5,000 particles were released in each 10° × 10° box. During the campaign, these calculations were made for a larger area at higher altitudes to reflect the larger range of the Global Hawk. The horizontal resolution of the Met Office operational model was 25 km in early 2014.

An example is shown in Fig. 1 for three altitude ranges (12–14, 14–16, and 16–18 km). Each point is the end point of each parcel of air that had crossed below 1 km in the preceding 12 days. For graphical clarity, only a fraction of the trajectories are shown at each level. Thus, strong, predicted low-level influence is indicated by a high percentage in each box (shown by the number), and at a given level by the denser clouds. These maps were routinely checked against flight plans for the Global Hawk and the GV to ensure that a wide range of low-level influences was sampled. In general, most flight plans met these criteria as a result of the proximity of the aircraft to the main convective region.

FAAM BAe-146 aircraft. The FAAM BAe-146 has a science payload of up to 4 tons (~3630 kg) devised

Table 2. Measurements made at the ARM site at Manus during CAST. Information about the meteorological measurements from Manus can be found online (www.arm.gov/sites/twp/C1/instruments).

Species (parameter)	Method/instrument details	Operation	Precision, accuracy	Affiliation; reference
O_3 (profile)	Ozonesonde, ENSCI model Z from DMT	Daily	See Newton et al. (2016)	University of Manchester, NCAS; Newton et al. (2016)
O_3 (surface)	Thermo-49 analyzer	Continuous (10 s)	±1 ppbv, precision limited	NCAS, Atmospheric Measurement Facility
CO_2, CH_4	Picarro G2401 CRDS analzser	Continuous (5 s)	CO_2 precision 0.05%, accuracy 0.05% (±1 std dev); CH_4 precision 0.05%, accuracy 0.1% (±1 std dev)	University of Cambridge; Crosson (2008)
Halocarbons ($CHBr_3$, $CHBr_2Cl$, CH_3I, CH_2ICl, C_2Cl_4)	Custom-built GC-ECD	Continuous (50 min)	Species dependent, typically 0.1–1 pptv	University of Cambridge; Gostlow et al. (2010), Robinson et al. (2014)

according to the objectives of a particular campaign. The chemical composition of the tropical atmosphere is the focus of CAST and this dictated the scientific payload. The chemical species and physical parameters measured on the FAAM aircraft, along with the instruments used, are summarized in Table 1. Trace gases with a wide range of atmospheric lifetimes, sources, and sinks were measured in order to provide information about the origin and fate of the air masses encountered, as well as about the atmospheric time scales involved. In many cases these species were also measured by the Global Hawk and/or the GV aircraft, giving good synergy between the three datasets. Understanding the distribution and chemistry of halogen species is a special focus for all three campaigns and this is reflected in the FAAM payload.

Whole air samples (WASs) were collected as described in Andrews et al. (2013). Analysis of WAS canisters was carried out in the aircraft hangar, usually within 72 h of collection. Two liters of sample air were preconcentrated using a thermal desorption unit (Markes Unity2 CIA-T) and analyzed with gas chromatography–mass spectrometry (GC-MS; Agilent 7890 GC, 5977 Xtr MSD). Halocarbons were quantified using a NOAA calibration gas standard. Dimethylsulfide was quantified using a secondary standard prepared and referenced to a primary [Korea Research Institute of Standards and Science (KRISS)] standard. The full method is detailed in Andrews et al. (2013, 2016).

Measurements of a subset of halocarbons and other volatile organic compounds (VOCs) were made in flight using a new thermal desorption (TD) GC-MS system. A 1-L sample of air, drawn from a window blank inlet, pressurized to 2.5 atm (1 atm = 101,325 Pa), and dried using a multicore countercurrent nafion drier, was alternately preconcentrated or analyzed from two parallel adsorption traps (Tenax TA) of a two-channel TD system (Markes International, model TT 24/7). Analyses were refocused at the head of the column using liquid CO_2 prior to separation (10 m, 180-μm inner diameter, 1-μm film, Restek RTX502.2 column; 40°–150°C at 40°C min^{-1}) by GC (Agilent 6850) and detection by electron impact MS single-ion monitoring (Agilent 5975C), calibrated preflight against the WAS gas standard (NOAA, SX-3581). The instrument temporal resolution, and associated sample integration period, was 5 min.

The chemical ionization mass spectrometer (CIMS) from the Georgia Institute of Technology was configured similarly to previous deployments (Le Breton et al. 2012, 2013). The I^- ionization scheme was used to detect inorganic halogens, carboxylic acids, HCN, and other trace species. For CAST, the CIMS made simultaneous measurements of BrO, BrCl, Br_2, and HOBr. The 1-Hz data were averaged to 30 s for analysis. Precampaign and postflight laboratory calibrations were used relative to in-flight formic acid calibrations to quantify the sensitivities and limits of detection for the inorganic halogens, similar to that used for dinitrogen pentoxide (Le Breton et al. 2014). The sensitivities ranged from 1 to 50 ion counts per part per trillion per second (ppt^{-1} s^{-1}) determined by in-flight and postcampaign calibrations. The limits of detection for species varied from 0.36 to 37 ppt for 30-s-averaged data. (All mixing ratios given in this paper are by volume.) An acid scrubber was used to quantify the background signal in the instrument and inlet line.

A broadband cavity-enhanced absorption spectrometer (BBCEAS) was adapted to measure input/output (IO) in the 410–482-nm-wavelength region. No clear absorption feature was observable from spectra by eye with up to 100-s averaging, pointing to very low mixing ratios (<~0.5 ppt) of IO over the sampled area. When using averaged data, a small positive bias (~0.3 ppt) of IO was observed with respect to zero. These observations appear to support the existence of IO in the remote marine boundary layer at sub-ppt levels, but the limited sensitivity precludes robust identification of spatial gradients.

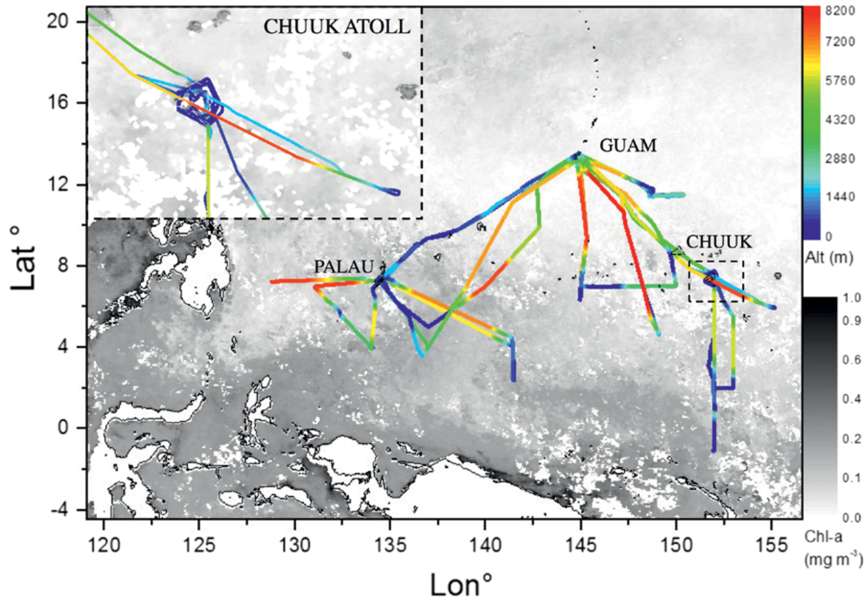

Fig. 2. Map of FAAM BAe-146 flight tracks during Jan–Feb 2014. The flight tracks are colored by altitude. The islands of Guam, Palau, and Chuuk are marked. The background shows Jan–Feb-averaged Chl-a concentrations in 2014, measured by the MODIS satellite [NASA Giovanni: Acker and Leptoukh (2007)]. The inset shows an enlarged area around Chuuk atoll.

Nitrous oxide was measured using chemiluminescence and NO_2 was quantified via a second channel, with NO_2 being converted to NO using a blue-light LED converter centered at 395 nm. The NO_2 mixing ratio is derived from the difference between the total NO_x and NO mixing ratios. The instrument is calibrated via addition of 5 standard cubic centimeters per minute (sccm) of known NO concentration to the ambient sample. The conversion efficiency of the LED converter is measured in each calibration using gas-phase titration of NO to NO_2 on addition of O_3. In-flight calibrations were conducted above the boundary layer to ensure stable low levels of NO_x with before- and after-flight calibrations made using an overflow at the inlet of zero-grade air. A more detailed description of a similar system can be found in Lee et al. (2009).

The level of O_3 was measured by an ultraviolet (UV) absorption photometer (Thermo Fisher, model 49C), traceable to the U.K. National Physical Laboratory primary ozone standard with an uncertainty of 2% and a precision of 1 ppb for 4-s measurements.

The CO level was measured by a vacuum UV fluorescence analyzer [Aero Laser GmbH, model AL5002; Gerbig et al. (1999)]. The instrument was calibrated in flight approximately every 45 min using a synthetic-air working standard (Air Liquide, ~500 ppb), traceable to the NOAA/Earth System Research Laboratory [Global Monitoring Division-Carbon Cycle Greenhouse Gases Group (GMD-CCGG)] surveillance standard and the World Meteorological Organization CO-scale X2004. The 1-Hz CO measurements have a 2% uncertainty and 3-ppb precision.

The CO_2 and CH_4 levels were measured by a cavity-enhanced IR absorption spectrometer (Los Gatos Research, Inc., fast greenhouse gas analyzer, model RMT-200). The instrument was customized for airborne operations (O'Shea et al. 2013), so CO_2 and CH_4 dry mole fractions can be linearized in flight using natural-air working standards, traceable to the World Meteorological Organization CO_2-scale X2007 and CH_4-scale X2004. The performance of the system is estimated from one standard deviation of all in-flight "target" calibration data. The 1-Hz measurement precisions are estimated at 0.7 ppm and 2.5 ppb for CO_2 and CH_4, respectively. Through the addition of all known uncertainties, we estimate a total accuracy of ±1.3 ppb for CH_4 and ±0.2 ppm for CO_2.

The Passive Cavity Aerosol Spectrometer Probe 100-X (PCASP), upgraded with the SPP-200 electronics package from Droplet Measurement Technologies (DMT), measures aerosol particles with nominal diameters of 0.1–3 μm. Light from a 0.6328-μm laser is scattered by the particles and a photodetector sums the forward (over solid angles subtended by 35°–120°) and backward (60°–145°) scattered light. The probe is

Table 3. Research flights made by the BAe-146 (FAAM) aircraft during the CAST project.			
Flight No.	**Date**	**Route**	**Flight description and observations**
B823	18 Jan 2014	Kota Kinabalu (KK)–Palau–Guam	Measurements on last part of leg from KK to Palau; flight mainly at low levels (in boundary layer) on Palau to Guam leg; O_3 and CO decreasing farther north (O_3: 30–12 ppb), higher (>35 ppb) above boundary layer (BL)
B824	22 Jan 2014	Guam–Guam	Heading southeast from Guam, 4000 m then 2000 m; flight aborted early because of technical problem with aircraft; GV followed ~30 min later; O_3 was 15 ppb near Guam, falling to 10 ppb at 7°S
B825	24 Jan 2014	Guam–Chuuk	Mixed altitudes (lowest 300 m), mainly within BL; O_3 dropping from 15 to 8 ppb toward Chuuk; CO was ~105 ppb on whole flight; southeast flow
B826	25 Jan 2014	Chuuk–Chuuk	Due south from Chuuk on 152°E to 2°N, then back on 153°E; started at 6000 m, then stepped down to 300 m; O_3 constant (~15 ppb) in BL, 25 ppb above BL; largely southeast flow in BL, west-northwest in free troposphere (FT)
B827	26 Jan 2014	Chuuk–Chuuk	Due south from Chuuk on 152°E to 1°N, then return on same track; in BL to 1°N, 4000 m on return north; well-mixed BL; 20 ppb O_3 to 1°N; BrO and CH_2Cl_2 observed; largely southeast flow in BL, west-northwest flow in FT
B828	26 Jan 2014	Chuuk–Guam	Circled atoll at 100 and 1500 m; then mixed altitude down to 300 m on way back to Guam; CO was 100 ppb around atoll in BL, O_3 was 15 ppb; O_3 was 10–13 ppb as headed north toward Guam
B829	29 Jan 2014	Guam–Palau	Mixed levels in BL down to 300 m; low O_3 (12 ppb) observed around island of Yap; easterly flow
B830	29 Jan 2014	Palau–Palau	Flight east along 7°N; mixed altitude down to 300 m; four stacked runs above each other at easterly end; profile of BrO observed on stacked runs—higher at surface; same CO and O_3 profiles at all levels, so BL was well mixed; 45 ppb O_3 and some NO_x (25 ppt) seen at 4000 m; higher N_2O at higher altitudes; largely southeast flow
B831	30 Jan 2014	Palau–Palau	Flight southeast into Indonesian airspace (4°30′N, 141°30′E), then due south to 3°N; mainly in BL, down to 300 m at most-southern point, where O_3 was 25–30 ppb; westerly flow, so some Asian outflow observed (CO < 100 ppb)
B832	30 Jan 2014	Palau–Guam	Low-level runs in BL crossing day–night terminator; 30 m in early part of flight before hitting low-level convection; above BL toward Guam; 15 ppb in O_3 during sunset, very constant as heading north; northwest flow
B833	1 Feb 2014	Guam–Guam	First part of day–night chemistry flights; stacked legs to east of Guam at 6000, 3000, 1500, 1000, and 300 m; northeast flow; followed GV for first half of flight (30 min behind)
B834	1 Feb 2014	Guam–Guam	Second part of day–night chemistry flights; stacked legs to east of Guam at 6000, 3000, 1500, 1000, and 300 m; northeast flow
B835	4 Feb 2014	Guam–Chuuk	Fast transit to Chuuk above BL; 25 ppb O_3, 85 ppb CO at 6000 m, and then O_3 lower as desending toward Chuuk (~13 ppb)
B836	4 Feb 2014	Chuuk–Chuuk	Heading south along 152°E at 7000 m, some low-level flying in BL to southernmost point (1°S) before maintaining intermediate height (2000–4000 m) back to Chuuk; 18 ppb O_3 above BL to 1°N; then profile down and less O_3 in BL (13 ppb), CO 70 ppb; at 1°S, O_3 was 9 ppb in northeast flow
B837	5 Feb 2014	Chuuk–Chuuk	Low-level flying in BL to southernmost point (~1°N, to complement B836), then climb back and return at ~5000 m; O_3 decreasing in BL as heading south; 20 ppb at 7°N, 11 ppb at 1°N; all in northeast flow
B838	6 Feb 2014	Chuuk–Chuuk	Round Chuuk atoll at three altitudes in BL (150, 500, and 1000 m); CO higher to east of islands (easterly flow); could be due to storms over the islands bringing elevated CO to the upwind side
B839	12 Feb 2014	Chuuk–Guam	Southeast of Guam at low level (500 m in BL), then above BL (5000 m) before descending down at lower levels in BL into Guam; O_3 spikes in profiles up to 7500 m (Asian outflow); 75 ppb seen at 7000 m

Table 3. Continued.

Flight No.	Date	Route	Flight description and observations
B840	13 Feb 2014	Guam–Palau	Starting in FT (~6500 m), then low nearer Palau (1500 m); heading to 4°N, 137°E before heading northwest; same region as GV and GH; O_3 was 30 ppb in FT and 12 ppb in BL; very stable; easterly flow
B841	14 Feb 2014	Palau–Palau	Flight to southwest of Palau with stacked legs in BL parallel to ATC boundary; O_3 was 15 ppb in BL; easterly flow
B842	14 Feb 2014	Palau–Guam	Reverse flight to B840; similar flow and O_3
B843	16 Feb 2014	Guam–Guam	South from Guam to 7°N, then east toward Chuuk before heading back to Guam; low-latitude parts at low altitudes (<1000 m in BL) under convective band; O_3 of 10–15 ppb in BL (E flow), elevated at higher levels (70–90 ppb), concurrent with elevated NO (30 ppt) (north flow)
B844	17 Feb 2014	Guam–Guam	South-southeast from Guam to fly under convective band (to 4°N) with low-level runs (<1000 m in BL); GV and GH flying nearby; layers of elevated O_3 and NO_x at 6000 m (westerly flow)
B845	17 Feb 2014	Guam–Guam	South from Guam to be west of convective band (to 6°N); low-level legs (<1000 m in BL) at southern end; layers of elevated O_3 and NO_x at ~6000 m (westerly flow)
B846	18 Feb 2014	Guam–Palau	Starting in FT (~6500 m), then low nearer Palau (1500 m); heading to 4°N, 137°E before turning northwest; same region as GV and GH; O_3: 30 ppb in FT, 12 ppb in BL; very stable; easterly flow
B847	18 Feb 2014	Palau–KK	Steady ascent toward KK; some Asian outflow observed on initial ascent (CO: ~140 ppb); westerly flow

canister mounted under the wing and was operated at 1 Hz. The instrument was calibrated for particle size before and after the campaign. Uncertainties exist in both the sizing and the counting of particles and these are discussed, along with the calibration procedure, in Rosenberg et al. (2012).

The DMT Cloud Droplet Probe (CDP; Lance et al. 2010) was flown on the same under-wing pylon as the PCASP. The CDP is an open-path instrument that measures the forward-scattered light (over solid angles nominally subtended by 1.7°–14°) from the 0.658-μm incident laser beam. Particles are assigned to 1 of 30 size bins over the nominal size range 3–50 μm. Calibration with certified diameter glass beads was carried out before each flight (Rosenberg et al. 2012). The sample rate of the CDP was the same as for the PCASP, 1 Hz.

Manus. Observations started at the ARM climate facility on Manus during October 1996 (Mather et al. 1998) and continued until August 2014. These observations provided the basis for many studies of the climate in the west Pacific (e.g., Long et al. 2013 and references therein). In February 2014, a suite of ground-based instruments was deployed as part of CAST to make measurements of ozone (ground and profile), short-lived halocarbons, carbon dioxide, carbon monoxide, and methane. The instruments used are now described and are also summarized in Table 2.

Ozone profiles were measured using ozonesondes. Air is pumped through a potassium–iodine (KI) solution in a cathode half-cell, with two electrons produced for each ozone molecule; the cell current is directly proportional to the flow of ozone through the cell. Ozonesondes have a typical response time of about 1 min at the tropopause level, with a precision of a few parts per billion. In the TTL the accuracy of the measurement is dominated by the background current (Newton et al. 2016 and references therein). Simultaneously, vertical profiles of temperature, humidity, wind, and pressure were measured with Vaisala RS92 radiosondes.

Ground-level ozone was measured by a Thermo-Electric Corporation TE49C, which is a dual-channel ultraviolet photometer measuring ozone through absorption of radiation at 254 nm. The incoming airstream is split between two identical cells, with a scrubber removing ozone from one of the streams. The TE49C provides a measurement every 10 s and has a 20-s response time.

Ground-level trace-gas concentrations were measured by a Picarro Cavity Ring-Down Spectrometer G2401 (CRDS; Crosson 2008). The sample air inlet was at about 8 m above ground level with a rain cover and a

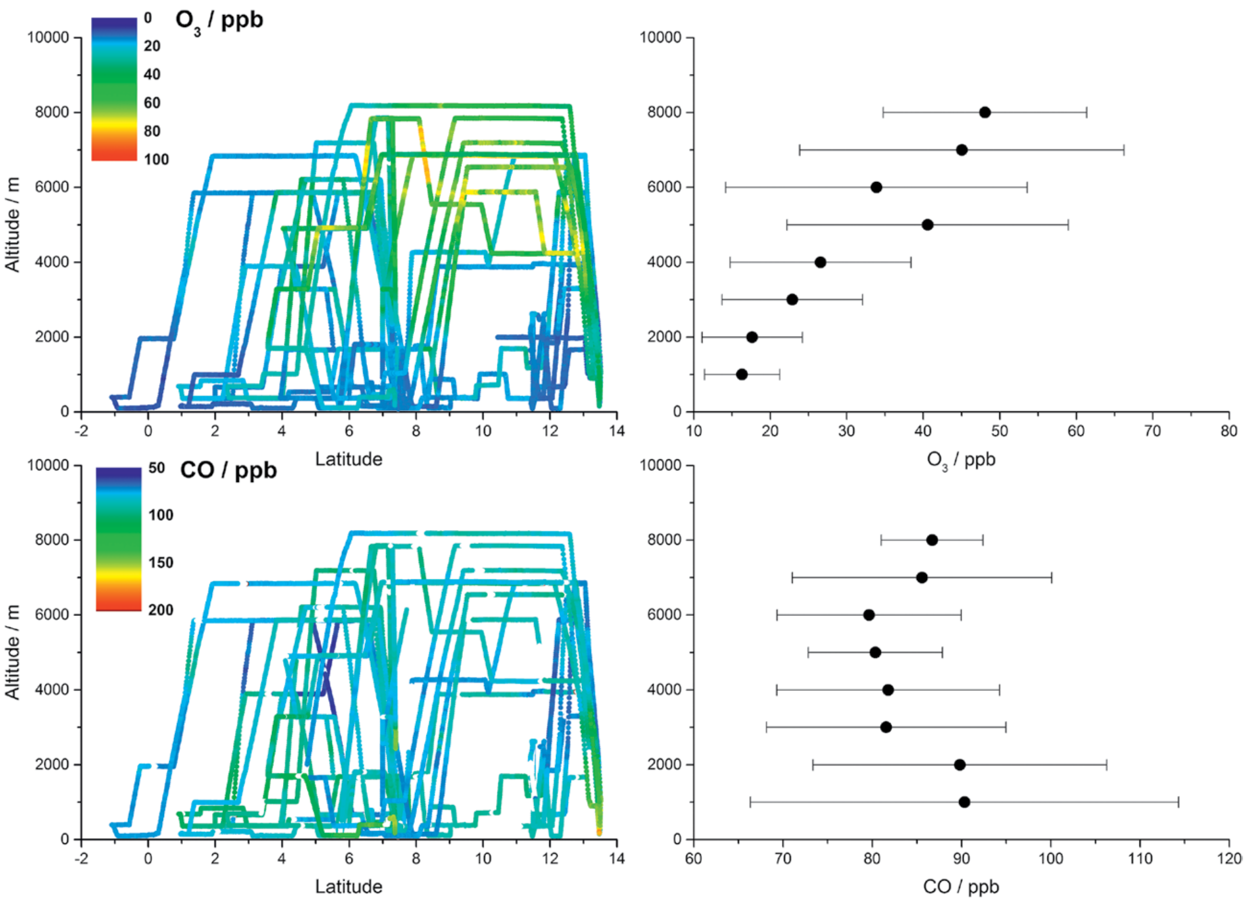

Fig. 3. (top left) Ozone and (top right) carbon monoxide mixing ratios measured during all CAST flights as a function of latitude and altitude. (right) The means and associated two standard deviations of ozone and carbon monoxide are shown as a function of altitude. See text and Table 1 for instrumental details.

2-μm particulate filter. Water vapor in the instrument was kept below 1.5 ppm and was controlled by passing the sample flow (~250 mL min^{-1}) through a chiller at approximately 5°C and then through a desiccant-based nafion drier. CO_2 and CH_4 concentrations were recorded every 5 s, with precisions of ~1 and ~200 ppb, respectively. Calibrations were achieved using a target gas (CH_4, 2024 ppb; CO_2, 390 ppm) measured every 2 days for 10 min with low and high calibration runs on intermediate days [low (high): CH_4, 1919 (2736) ppb; CO_2, 360 (495) ppm]. The calibration gases are linked to the NOAA–WMO calibration scale.

Surface concentrations of short-lived halocarbons were measured using a μDirac instrument, a gas chromatograph with an electron capture detector (GC-ECD) based on an instrument described in Gostlow et al. (2010) but with a 10-m separation column. The instrument sampled ambient air from the roughly 8-m-high mast, with a 10–20 mL min^{-1} flow dried using a counterflow nafion drier. Calibration runs, using a NOAA/ESRL air cylinder spiked with the target compounds, were conducted regularly (every three samples). The calibration volumes ranged from 3 to 50 mL to allow correction for drifts in instrument sensitivity and linearity. Measurement precision is species dependent, typically 2%–10% (plus or minus one standard deviation), with accuracy in the range of 5%–10% (plus or minus one standard deviation).

OVERVIEW OF MEASUREMENTS. The FAAM BAe-146 made a total of 25 science flights totaling 90 flight hours during the CAST deployment in the west Pacific (Fig. 2). Brief summaries of the flights are given in Table 3. The flight tracks are shown in Fig. 2, with the altitude represented by the color of the line. The large majority of the flights were below 5-km altitude, with a significant fraction in the marine boundary layer (below about 1 km), with good coverage between 2°S and 14°N and 130° and 160°E.

The vertical distribution of the science flights can also be seen in Fig. 3, which shows O_3 and CO concentrations as a function of altitude and latitude. In general, lower O_3 values are found in the marine boundary layer and at lower latitudes, while high values are found at higher altitudes and at higher latitudes. There is no obvious correlation with CO. However, when the O_3 and CO data are plotted against each other (Fig. 4), a bimodal relationship emerges. Further, the lower ozone values (10–40 ppb) occur when the relative humidity is high (Fig. 4, top). This finding reinforces that of Pan et al. (2015), who report this bimodality throughout the altitude range covered by the NCAR GV, with a background mode of nearly constant (~20 ppb) values throughout the troposphere and a secondary mode of higher ozone (~35–95 ppb) in layers with lower relative humidity. The previously reported S-shaped mean profile (Folkins et al. 2002) results from averaging the two modes.

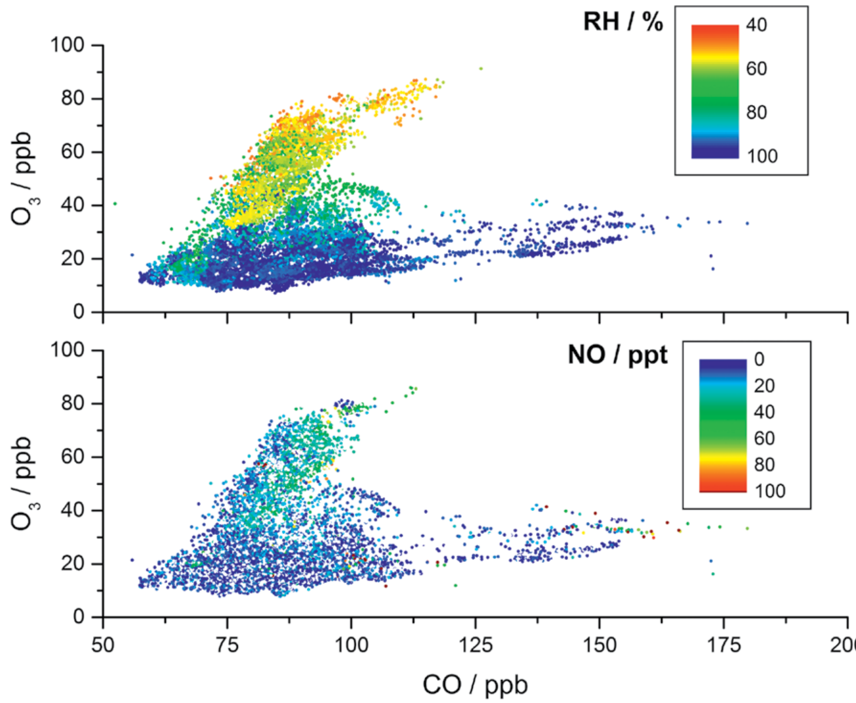

Fig. 4. Plots of O_3 against CO colored by (bottom) NO and (top) relative humidity (10-s-averaged data).

The CAST measurements (Fig. 4) show that high ozone and lower relative humidity often occurs with higher NO concentrations and does not occur with low CO concentrations. Preliminary analysis of the high NO measurements indicates that the air masses encountered had previously been in regions close to anthropogenic activities and/or biomass burning. For example, the MACC forecasts show the transport of biomass burning and Southeast Asian tracers to the west Pacific. The possible role of biomass burning has been thoroughly investigated by Anderson et al. (2016) using CAST and CONTRAST measurements. The presence of HCN, CH_3CN, and other tracers in the high-ozone levels is explained by biomass-burning plumes, which are convectively lofted into the free troposphere undergoing dehydration during the convection. As this air descends, its relative humidity drops and ozone is produced photochemically.

The $CHBr_3$ concentrations measured with the Whole Air Sampler and the onboard GC-MS are shown in Fig. 5. In general the values are low, with even the higher values not far above the background values seen in this region (Brinckmann et al. 2012). The lower amounts of $CHBr_3$ were encountered out of the boundary layer (Fig. 4b). The background in Fig. 2 shows that the chlorophyll-a (Chl-a) concentrations in the surface waters of the west Pacific were low during this period. Higher Chl-a values are seen in the shallower waters approaching the islands of the Maritime Continent. The lagoon inside Chuuk atoll is relatively shallow (<60 m) and is embedded in much deeper ocean waters. It has a circumference of about 200 km and an area of about 3000 km^2. If halocarbons are emitted preferentially in shallow waters (Carpenter et al. 2009), then it should be discernible as an emission hotspot. The influence of short-lived halocarbon emissions from shallower waters was investigated during the FAAM flights by circling Chuuk atoll at low altitudes. The inset in Fig. 5a shows the $CHBr_3$ observed on these flights as well as the instantaneous wind speed observed by the FAAM aircraft. Higher concentrations of $CHBr_3$ (red) are found when air has previously passed over the atoll, indicating that the atoll is a source of $CHBr_3$.

The NAME model driven by Met Office analyzed fields has been used to interpret the $CHBr_3$ and other brominated VSLS measurements made near the tropopause on the Global Hawk in the east Pacific during 2013 and the west Pacific during 2014 (Navarro et al. 2015). The approach is similar to the forecast information produced during the campaign (see above). They find that the majority of air recently injected into the TTL had come from the west Pacific in both years with similar amounts, approximately 6 (4–9) ppt, of

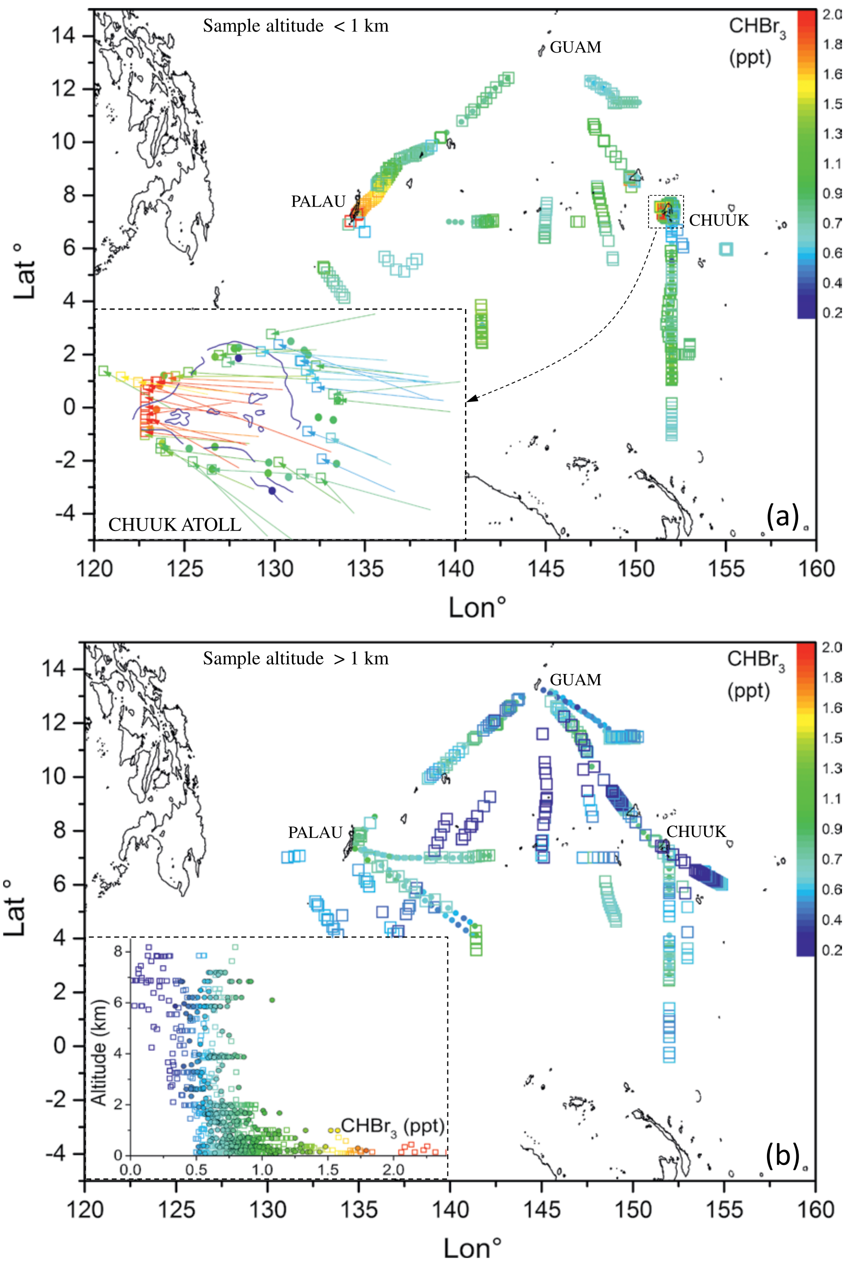

Fig. 5. $CHBr_3$ mixing ratios (colors) sampled by the FAAM aircraft during CAST using the whole air sampler (squares) and the onboard GC-MS (circles). (a) All measurements made at altitudes less than 1 km. The enlarged inset shows the values around the Chuuk atoll. The lines associated with each measurement in the inset indicate the instantaneous wind speed measured by the aircraft. (b) The measurements at altitudes greater than 1 km. The inset shows the vertical profile of all measurements.

combined organic and inorganic bromine derived from brominated VSLS.

At the ARM facility in Manus, $CHBr_3$ was also observed (Fig. 5). The median value in this period was 0.81 ppt, about half that previously observed at a coastal site in Malaysian Borneo (Robinson et al. 2014) and similar to the values observed on the FAAM aircraft (Fig. 4). A strong diurnal cycle is seen in early February in several trace gases measured at Manus with increased nocturnal amounts, providing evidence for local nighttime sources of CO_2, CH_4, $CHBr_3$, and CH_3I. This diurnal pattern of behavior was seen from 3 to 12 February when the winds were low and a stable boundary layer was able to form. Before and after this period winds were higher and the nighttime buildup was much less.

Together, the $CHBr_3$ observations appear to be consistent with past work focused on Southeast Asia. Elevated levels are frequently observed close to coasts (e.g., Pyle et al. 2011) or above shallow waters, but measurements collected a relatively small distance away (less than a typical global model grid cell) rarely contain above-background levels of $CHBr_3$. This suggests that coasts are not a large source in a regional/global sense (as found by Ashfold et al. 2014), and for coastal $CHBr_3$ emissions to contribute significantly to the TTL and stratosphere would require collocation of convection (Russo et al. 2015).

Ground-based ozone at Manus showed decreases at night in the quiescent period from a peak daytime value of 10 to <5-ppb levels which is consistent with oxidative uptake to the local vegetation (Fig. 6). This is the only time such low values of ozone were seen in CAST. In the absence of local sources, C_2Cl_4 is a good tracer of large-scale transport, and its concentrations during this period were generally in the range 1–1.5 ppt, which is typical of results seen in the clean west Pacific (Ashfold et al. 2015). Manus was mainly influenced by flow from the north throughout this period.

A total of 39 ozonesondes were launched from Manus in February 2014, with 34 sondes providing good ozone profiles (Fig. 7a; Newton et al. 2016). These measurements are most difficult in the tropics as the ozone concentrations are low, so that any error in estimating the background current is important. Particular attention was therefore paid to measurements of the background current, leading to recommendations for changes to the standard operation procedures used in the sonde preparation. Support for this approach is provided by good agreement in a coordinated ozonesonde–GV flight (see Fig. 14 in Pan et al. 2017). The ozone measurements are shown in Fig. 7 alongside the corresponding MACC 1- and 4-day forecasts. The forecasts predicted the main characteristics of the observations such as increased ozone at about 400 hPa from 14 to 16 February and the low concentrations near the TTL from 19 to 23 February. The minimum reproducible ozone concentration measured in the TTL was 12 ppb, consistent with the minimum of 13 ppb measured by the GV during CONTRAST (Pan et al. 2017).

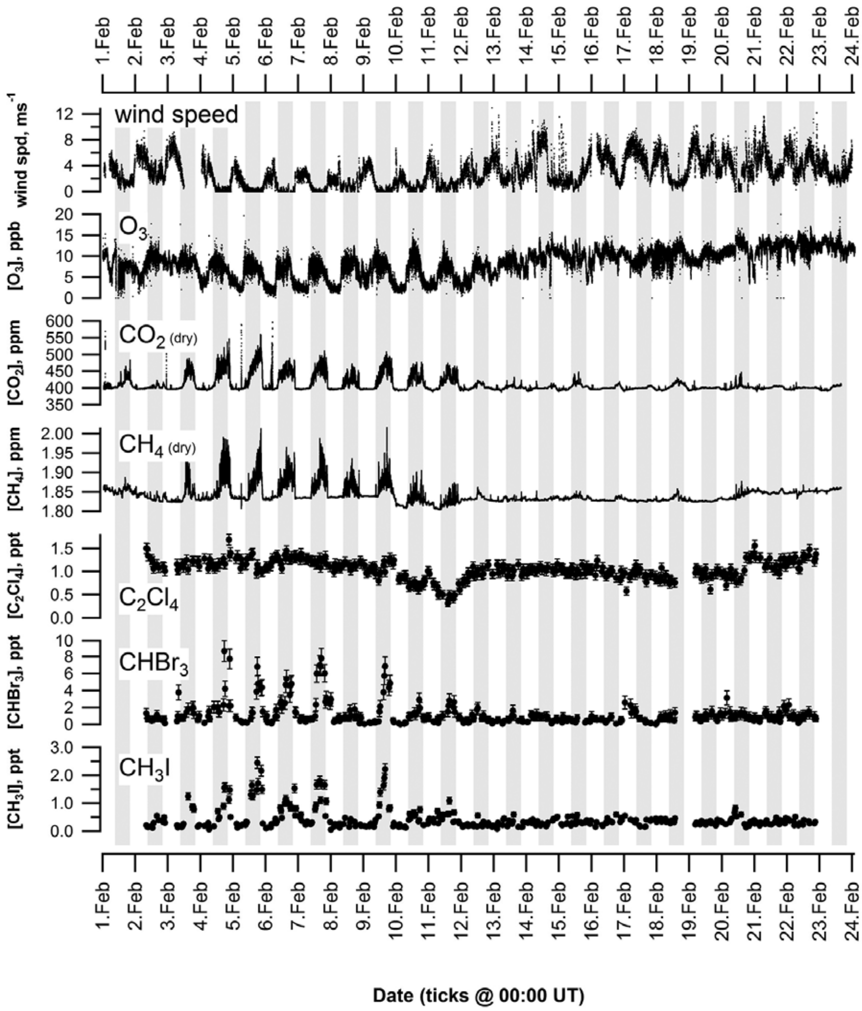

Fig. 6. Surface observations of (top to bottom) wind, O_3, CO_2, CH_4, C_2Cl_4, $CHBr_3$, and CH_3I at the ARM facility on Manus from 1 to 24 Feb 2014. The time shown along the *x* axis is universal time. The shading indicates the local time, with the darker bands representing nighttime.

New technology developments. As part of the collaboration with ATTREX, three new developments were included in CAST: two instruments for use on the Global Hawk, the Aerosol–Ice–Interface Transition Spectrometer (AIITS) and the Greenhouse Gas Observations in the Stratosphere and Troposphere (GHOST), along with a software tool, Real-Time Atmospheric Science Cluster Analysis (RASCAL), designed to assist aircraft scientists by performing real-time data analysis during flights. The two new instruments were flown for a total of 40 h during one test flight and two science flights in February–March 2015 from the NASA Armstrong Flight Research Center, Edwards Air Force Base, California. They were part of a payload that also included Hawkeye, the NOAA H_2O and O_3 instruments, the Global Hawk Whole Air Sampler (GWAS), and the Microwave Temperature Profiler (MTP) (see Jensen et al. 2017 for more details).

AIITS was designed to probe different cirrus regimes in the TTL in order to understand fundamental nucleation and sublimation processes influencing the stratospheric water budget and fluxes, as well as the potential impact of biomass burning on cirrus ice crystal activation and growth. It is the next instrument in the Small Ice Detector (SID) family (Hirst et al. 2001; Kaye et al. 2008). AIITS acquires 2D forward-scattering patterns from particles in the size range from about one to a few hundred micrometers and can measure the depolarization in backward and forward scattering. The patterns allow quantification

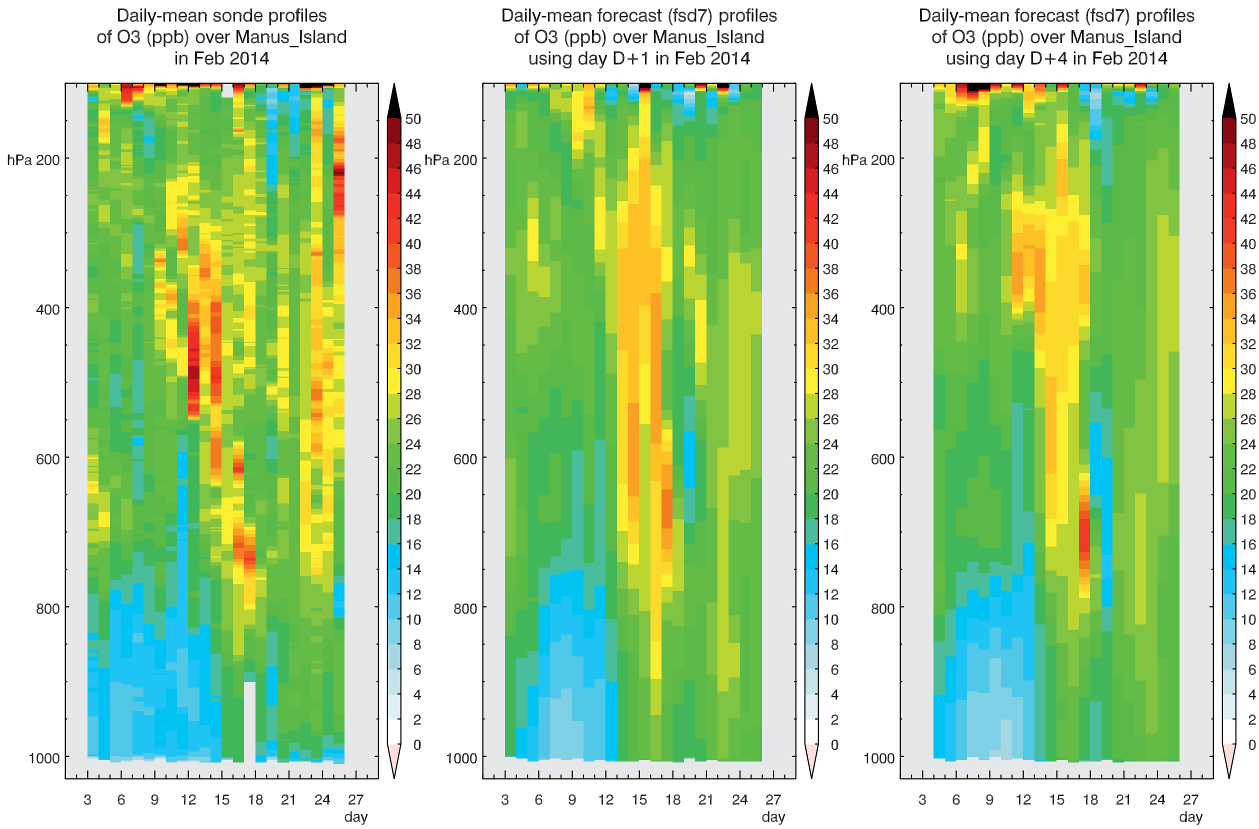

Fig. 7. (left) Daily observed ozone profile in Manus and corresponding MACC forecasts with lead times of (center) 1 and (right) 4 days.

of the phase, habit, and fine surface features of large aerosol and small ice crystals in the size range 2–100 μm (Cotton et al. 2010; Ulanowski et al. 2014). Unique results were obtained by AIITS during cirrus penetrations at 16.5 km and at temperatures down to -80°C (Fig. 8). These revealed a transition to smooth quasi-spherical ice particle regimes in specific regions of TTL layers in response to changing supersaturation regimes. The impact on the radiative scattering properties of cirrus in these regimes is being investigated.

GHOST is a novel grating spectrometer designed for remote sensing of greenhouse gases from aircraft (Humpage et al. 2014). It measures spectrally resolved shortwave-infrared radiance across four spectral bands from 1.27 to 2.3 μm, with a spectral resolution between 0.1 and 0.3 nm. An optical gimbal underneath the aircraft is programmed to pass solar radiation reflected from the ocean surface through a fiber optic bundle into the spectrometer with a single grating and detector for all four bands. The bands are chosen to include absorption bands for CO_2 and CH_4 as well as CO, H_2O, and O_2; O_2 is used to infer information on the scattering contributions toward the measured light. The third Global Hawk flight of the CAST/ATTREX campaign targeted the overpasses of two greenhouse gas observing satellites during clear-sky conditions over the eastern Pacific (Fig. 9): the NASA Orbiting Carbon Observatory (OCO-2) and the Japan Aerospace Exploration Agency (JAXA) Greenhouse Gas Observing Satellite (GOSAT). This Global Hawk flight therefore provides a very useful validation dataset for these satellites, since they both make greenhouse gas measurements using a spectral range similar to that of GHOST.

As real-time data becomes increasingly available, mission scientists are faced with a potentially overwhelming data torrent, from which they are required to find the information on which to base decisions. At present, mission scientists often focus on a subset of the data stream, limiting the depth of the analysis that can be carried out. As part of CAST, a new software framework, RASCAL, has been developed based on recent developments in arbitrarily shaped cluster detection algorithms (Hyde and Angelov 2015). It interfaces intuitively with mission scientist expert knowledge and provides real-time on-the-fly cluster and anomaly detection (i.e., for real-time diagnosis of structures such as those presented in Fig. 4, for example, but tested simultaneously across many chemical "dimensions"). The data stream can

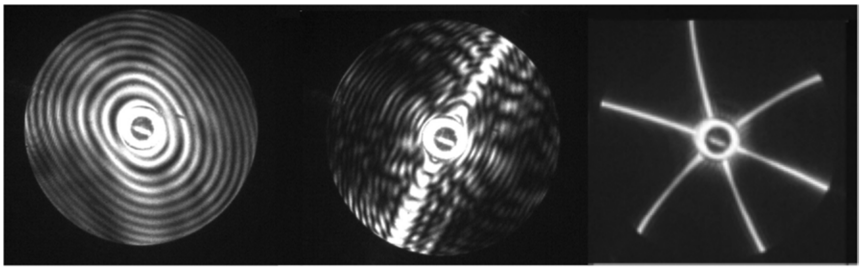

Fig. 8. AIITS scattering patterns recorded from ice particles in the upper troposphere–lower stratosphere (UTLS), at altitudes of about 16 km and temperatures of about −80°C. The pictures are indicative of (left) a smooth quasi-spherical ice particle, (center) a columnar crystal, and (right) a pristine hexagonal plate.

be separated in real time, without a priori assumptions about parameter relationships, to reveal different data groups and hence isolate specific regions of interest that can be revisited virtually postflight. In combination with the expert knowledge of the mission scientists, support tools like RASCAL have the potential to be used on many research aircraft, potentially adding significant value to the results achieved in field measurement campaigns.

SUMMARY. Based in Guam as part of a joint deployment with the NASA ATTREX Global Hawk and the NSF CONTRAST GV, the FAAM research aircraft deployment during CAST has provided an excellent characterization of the lower-tropospheric atmospheric composition in the tropical warm pool region. The majority of the FAAM aircraft flights were below 5-km altitude, and a significant fraction was in the marine boundary layer with good coverage from 2°S to 14°N and from 130° to 160°E. A suite of organic and inorganic halogen compounds was measured, with the bromine-containing species being particularly well covered.

Ground-based measurements were made at the ARM facility on Manus Island, Papua New Guinea, during February 2014. These measurements characterize the tropospheric composition just south of the equator in a region inaccessible to the FAAM aircraft in this deployment. The Manus ozonesonde measurements are a valuable resource, providing a good picture of the vertical distribution of ozone in the tropical warm pool region during February with a minimum ozone concentration in the TTL of 12 ppb.

These measurements are being interpreted by CAST scientists in conjunction with measurements from ATTREX and CONTRAST using a range of modeling and data analysis approaches. The CAST data are stored at the British Atmospheric Data Centre (http://badc.nerc.ac.uk/), and interested parties are encouraged to use them for their own studies. All users are strongly encouraged to involve the responsible instrument scientists in these studies in order to gain insight into the strengths and weaknesses of these data.

Never before has the atmosphere over the west Pacific been observed in such detail, particularly the chemical composition, with three aircraft covering all altitudes from 0 to 20 km. New insights are starting to emerge with a much improved understanding of the tropical ozone distribution (Pan et al. 2015; Anderson et al. 2016; Newton et al. 2016). These findings will be underpinned by advances in the understanding of halogen

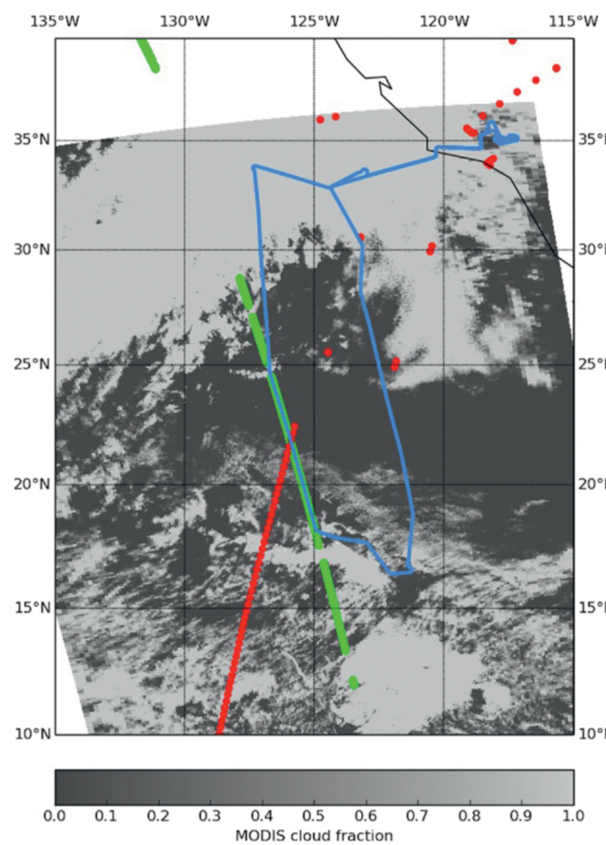

Fig. 9. Flight path of the NASA Global Hawk on 10 Mar 2015 (blue). The OCO-2 (green) and GOSAT (red) soundings are shown and coincide temporally with the flight leg between 25°N, 127°W and 18°N, 125°W. MODIS cloud fraction data (see gray scale bar; Platnick et al. 2015) coincident with the OCO-2 overpass at 2140 UTC shows the largely cloud-free conditions encountered during this leg of the flight.

distribution (Navarro et al. 2015) and chemistry building on the new tropospheric halogen measurements and modeling (Sherwen et al. 2016). Such research will lead to a much greater quantitative understanding of the role of a) VSLS reaching the stratosphere and b) how halogen chemistry affects tropospheric ozone over the tropical oceans. Similar advances can be expected with respect to transport and dynamics, the role of cirrus clouds in climate, and dehydration of the stratosphere. The benefits of this unique, coordinated campaign are just starting to become clear.

ACKNOWLEDGMENTS. CAST is funded by NERC and STFC, with Grants NE/ I030054/1 (lead award), NE/J006262/1, NE/J006238/1, NE/J006181/1, NE/J006211/1, NE/J006061/1, NE/J006157/1, NE/J006203/1, NE/J00619X/1, and NE/J006173/1. NRPH was supported by a NERC Advanced Research Fellowship (NE/G014655/1). PIP acknowledges his Royal Society Wolfson Research Merit Award. The BAe-146-301 Atmospheric Research Aircraft is flown by Directflight Ltd, and managed by the Facility for Airborne Atmospheric Measurements, which is a joint entity of the Natural Environment Research Council and the Met Office. The authors thank the staff at FAAM, Directflight, and Avalon Aero, who worked so hard toward the success of the aircraft deployment in Guam, especially for their untiring efforts when spending an unforeseen nine days in Chuuk. We thank the local staff at Chuuk and Palau, as well as the authorities in the Federated States of Micronesia for their help in facilitating our research flights. Special thanks go to the personnel associated with the ARM facility at Manus, Papua New Guinea, without whose help the ground-based measurements would not have been possible. Thanks to the British Atmospheric Data Centre (BADC) for hosting our data and the NCAS Atmospheric Measurement Facility for providing the radiosonde and ground-based ozone equipment. Chlorophyll-a data used in Fig. 1 were extracted using the Giovanni online data system, maintained by the NASA GES DISC. We acknowledge the MODIS mission scientists and associated NASA personnel for the production of this dataset. Finally we thank many individuals associated with the ATTREX and CONTRAST campaigns for their help in the logistical planning, and we would like to single out Jim Bresch for his excellent and freely provided meteorological advice.

REFERENCES

Acker, J. G., and G. Leptoukh, 2007: Online analysis enhances use of NASA Earth science data. *Eos, Trans. Amer. Geophys. Union,* **88**, 14–17, doi:10.1029/2007EO020003.

Anderson, D. C., and Coauthors, 2016: A pervasive role for biomass burning in tropical high ozone/low water structures. *Nat. Commun.,* **7,** 10267, doi:10.1038/ncomms10267.

Andrews, S. J., C. E. Jones, and L. J. Carpenter, 2013: Aircraft measurements of very short-lived halocarbons over the tropical Atlantic Ocean. *Geophys. Res. Lett.,* **40,** 1005–1010, doi:10.1002/grl.50141.

——, and Coauthors, 2016: A comparison of very short lived halocarbon (VSLS) and DMS aircraft measurements in the tropical west Pacific from CAST, ATTREX and CONTRAST. *Atmos. Meas. Tech.*, **9**, 5213–5225, doi:10.5194/amt-9-5213-2016.

Ashfold, M. J., N. R. P. Harris, E. L. Atlas, A. J. Manning, and J. A. Pyle, 2012: Transport of short-lived species into the tropical tropopause layer. *Atmos. Chem. Phys.,* **12,** 6309–6322, doi:10.5194/acp-12-6309-2012.

——, ——, A. J. Manning, A. D. Robinson, N. J. Warwick, and J. A. Pyle, 2014: Estimates of tropical bromoform emissions using an inversion method. *Atmos. Chem. Phys.,* **14,** 979–994, doi:10.5194/acp-14-979-2014.

——, and Coauthors, 2015: Rapid transport of East Asian pollution to the deep tropics. *Atmos. Chem. Phys.,* **15,** 3565–3573, doi:10.5194/acp-15-3565-2015.

Brinckmann, S., A. Engel, H. Bönisch, B. Quack, and E. Atlas, 2012: Short-lived brominated hydrocarbons—Observations in the source regions and the tropical tropopause layer. *Atmos. Chem. Phys.,* **12,** 1213–1228, doi:10.5194/acp-12-1213-2012.

Carpenter, L. J., C. E. Jones, R. M. Dunk, K. E. Hornsby, and J. Woeltjen, 2009: Air–sea fluxes of biogenic bromine from the tropical and North Atlantic Ocean. *Atmos. Chem. Phys.,* **9,** 1805–1816, doi:10.5194/acp-9-1805-2009.

——, and Coauthors, 2014: Ozone-depleting substances (ODSs) and other gases of interest to the Montreal Protocol. *Scientific Assessment of Ozone Depletion: 2014*, A. Engel and S. A. Montzka, Eds., Global Ozone Research and Monitoring Project Rep. 55, World Meteorological Organization, 1–101. [Available online at www.wmo.int/pages/prog/arep/gaw/ozone_2014/documents/Full_report_2014_Ozone_Assessment.pdf.]

Cotton, R., S. Osborne, Z. Ulanowski, E. Hirst, P. H. Kaye, and R. Greenaway, 2010: The ability of the Small Ice Detector (SID2) to characterize cloud particle and aerosol morphologies obtained during flights of the FAAM BAe-146 research aircraft. *J. Atmos. Oceanic Technol.,* **27,** 290–303, doi:10.1175/2009JTECHA1282.1.

Crosson, E. R., 2008: A cavity ring-down analyzer for measuring atmospheric levels of methane, carbon dioxide, and water vapor. *Appl. Phys. B,* **92,** 403–408, doi:10.1007/s00340-008-3135-y.

Flemming, J., and Coauthors, 2015: Tropospheric chemistry in the Integrated Forecasting System of ECMWF.

Geosci. Model Dev., **8,** 975–1003, doi:10.5194/gmd-8-975-2015.

Folkins, I., C. Braun, A. M. Thompson, and J. Witte, 2002: Tropical ozone as an indicator of deep convection. *J. Geophys. Res.,* **107,** 4184, doi:10.1029/2001JD001178.

Fueglistaler, S., A. E. Dessler, T. J. Dunkerton, I. Folkins, Q. Fu, and P. W. Mote, 2009: Tropical tropopause layer. *Rev. Geophys.,* **47,** RG1004, doi:10.1029/2008RG000267.

Gerbig, C., S. Schmitgen, D. Kley, A. Volz-Thomas, K. Dewey, and D. Haaks, 1999: An improved fast-response VUV resonance flourescence CO instrument. *J. Geophys. Res.,* **104,** 1699–1704, doi:10.1029/1998JD100031.

Gettelman, A., M. L. Salby, and F. Sassi, 2002: Distribution and influence of convection in the tropical tropopause region. *J. Geophys. Res.,* **107**, doi:10.1029/2001JD001048.

Gostlow, B., and Coauthors, 2010: Micro-DIRAC: An autonomous instrument for halocarbon measurements. *Atmos. Meas. Tech.,* **3,** 507–521, doi:10.5194/amt-3-507-2010.

Heyes, W. J., G. Vaughan, G. Allen, A. Volz-Thomas, H.-W. Pätz, and R. Busen, 2009: Composition of the TTL over Darwin: Local mixing or long-range transport? *Atmos. Chem. Phys.,* **9,** 7725–7736, doi:10.5194/acp-9-7725-2009.

Hirst, E., P. H. Kaye, R. S. Greenaway, P. Field, and D. W. Johnson, 2001: Discrimination of micrometresized ice and super-cooled droplets in mixed-phase cloud. *Atmos. Environ.,* **35,** 33–47, doi:10.1016/S1352-2310(00)00377-0.

Hopkins, J. R., K. A. Read, and A. C. Lewis, 2003: A two column method for long-term monitoring of non-methane hydrocarbons (NMHCs) and oxygenated volatile organic compounds. *J. Environ. Monit.,* **5,** 8–13, doi:10.1039/b202798d.

Humpage, N., and Coauthors, 2014: GreenHouse Observations of the Stratosphere and Troposphere (GHOST): A novel shortwave infrared spectrometer developed for the Global Hawk unmanned aerial vehicle. *Proc. SPIE 9242, Remote Sensing of Clouds and the Atmosphere XIX and Optics in Atmospheric Propagation and Adaptive Systems XVII,* A. Comerón et al., Eds., International Society for Optical Engineering (SPIE Proceedings, Vol. 92420P), doi:10.1117/12.2067330.

Hyde, R., and P. Angelov, 2015: A new online clustering approach for data in arbitrary shaped clusters. *Proc. Second Int. Conf. on Cybernetics*, Gydnia, Poland, IEEE, 228–233, doi:10.1109/CYBConf.2015.7175937.

Ishijima, K., and Coauthors, 2010: Stratospheric influence on the seasonal cycle of nitrous oxide in the troposphere as deduced from aircraft observations and model simulations. *J. Geophys. Res.,* **115,** D20308, doi:10.1029/2009JD013322.

Jensen, E. J., and Coauthors, 2017: The NASA Airborne Tropical Tropopause Experiment (ATTREX): High-altitude aircraft measurements in the tropical western Pacific. *Bull. Amer. Meteor. Soc.,* **98**, 129–143, doi:10.1175/BAMS-D-14-00263.1.

Kaye, P. H., E. Hirst, R. S. Greenaway, Z. Ulanowski, E. Hesse, P. J. DeMott, C. Saunders, and P. Connolly, 2008: Classifying atmospheric ice crystals by spatial light scattering. *Opt. Lett.,* **33,** 1545, doi:10.1364/OL.33.001545.

Kennedy, O. J., and Coauthors, 2011: An aircraft based three channel broadband cavity enhanced absorption spectrometer for simultaneous measurements of NO_3, N_2O_5 and NO_2. *Atmos. Meas. Tech.,* **4,** 1759–1776, doi:10.5194/amt-4-1759-2011.

Lance, S., C. A. Brock, D. Rogers, and J. A. Gordon, 2010: Water droplet calibration of the Cloud Droplet Probe (CDP) and in-flight performance in liquid, ice and mixed-phase clouds during ARCPAC. *Atmos. Meas. Tech.,* **3,** 1683–1706, doi:10.5194/amt-3-1683-2010.

Le Breton, M., and Coauthors, 2012: Airborne observations of formic acid using a chemical ionization mass spectrometer. *Atmos. Meas. Tech.,* **5,** 3029–3039, doi:10.5194/amt-5-3029-2012.

——, and Coauthors, 2013: Airborne hydrogen cyanide measurements using a chemical ionisation mass spectrometer for the plume identification of biomass burning forest fires. *Atmos. Chem. Phys.,* **13,** 9217–9232, doi:10.5194/acp-13-9217-2013.

——, and Coauthors, 2014, The first airborne comparison of N_2O_5 measurements over the UK using a CIMS and BBCEAS during the RONOCO campaign. *Anal. Methods*, **6**, 9731–9743, doi:10.1039/c4ay02273d.

Lee, J. D., S. J. Moller, K. A. Read, A. C. Lewis, L. Mendes, and L. J. Carpenter, 2009: Year-round measurements of nitrogen oxides and ozone in the tropical North Atlantic marine boundary layer. *J. Geophys. Res.,* **114,** D21302, doi:10.1029/2009JD011878.

Lenschow, D. H., 1986: Aircraft measurements in the boundary layer. *Probing the Atmospheric Boundary Layer*, D. H. Lenschow, Ed., Amer. Meteor. Soc., 39–55.

Levine, J. G., P. Braesicke, N. R. P. Harris, N. H. Savage, and J. A. Pyle, 2007: Pathways and timescales for troposphere-to-stratosphere transport via the tropical tropopause layer and their relevance for very short lived substances. *J. Geophys. Res.,* **112,** D04308, doi:10.1029/2005JD006940.

——, ——, ——, and J. A. Pyle, 2008: Seasonal and inter-annual variations in troposphere-to-stratosphere transport from the tropical tropopause layer.

Atmos. Chem. Phys., **8,** 3689–3703, doi:10.5194/acp-8-3689-2008.

Liu, D., and Coauthors, 2015: The importance of Asia as a source of black carbon to the European Arctic during springtime 2013. *Atmos. Chem. Phys.,* **15,** 11 537–11 555, doi:10.5194/acp-15-11537-2015.

Long, C. N., and Coauthors, 2013: ARM research in the equatorial western Pacific: A decade and counting. *Bull. Amer. Meteor. Soc.,* **94,** 695–708, doi:10.1175/BAMS-D-11-00137.1.

Mather, J. H., T. P. Ackerman, W. E. Clements, F. J. Barnes, M. D. Ivey, L. D. Hatfield, and R. M. Reynolds, 1998: An Atmospheric Radiation and Cloud Station in the tropical western Pacific. *Bull. Amer. Meteor. Soc.,* **79,** 627–642, doi:10.1175/1520-0477(1998)079<0627:AARACS>2.0.CO;2.

Navarro, M. A., and Coauthors, 2015: Airborne measurements of organic bromine compounds in the Pacific tropical tropopause layer. *Proc. Nat. Acad. Sci.,* **112**, 13 789–13 793, doi:10.1073/pnas.1511463112.

Newton, R., G. Vaughan, H. M. A. Ricketts, L. L. Pan, A. J. Weinheimer, and C. Chemel, 2016: Ozonesonde profiles from the west Pacific warm pool: Measurements and validation. *Atmos. Chem. Phys.,* **16,** 619–634, doi:10.5194/acp-16-619-2016.

O'Shea, S. J., S. J.-B. Bauguitte, M. W. Gallagher, D. Lowry, and C. J. Percival, 2013: Development of a cavity-enhanced absorption spectrometer for airborne measurements of CH_4 and CO_2. *Atmos. Meas. Tech.,* **6,** 1095–1109, doi:10.5194/amt-6-1095-2013.

Pan, L. L., and Coauthors, 2015: Bimodal distribution of free tropospheric ozone over the tropical western Pacific revealed by airborne observations. *Geophys. Res. Lett.,* **42**, 7844–7851, doi:10.1002/2015GL065562.

——, and Coauthors, 2017: The Convective Transport of Active Species in the Tropics (CONTRAST) experiment. *Bull. Amer. Meteor. Soc.,* **98**, 106–128, doi:10.1175/BAMS-D-14-00272.1.

Petersen, G. N., and I. A. Renfrew, 2009: Aircraft-based observations of air–sea fluxes over Denmark Strait and the Irminger Sea during high wind speed conditions. *Quart. J. Roy. Meteor. Soc.,* **135,** 2030–2045, doi:10.1002/qj.355.

Platnick, S., and Coauthors, 2015: MODIS Atmosphere L2 Cloud Product (06_L2). NASA MODIS Adaptive Processing System, NASA Goddard Space Flight Center, accessed 23 October 2015, doi:10.5067/MODIS/MYD06_L2.006.

Pyle, J. A., and Coauthors, 2011: Bromoform in the tropical boundary layer of the Maritime Continent during OP3. *Atmos. Chem. Phys.,* **11,** 529–542, doi:10.5194/acp-11-529-2011.

Randel, W., and E. Jensen, 2013: Physical processes in the tropical tropopause layer and their roles in a changing climate. *Nat. Geosci.,* **6,** 169–176, doi:10.1038/ngeo1733.

Robinson, A. D., and Coauthors, 2014: Long-term halocarbon observations from a coastal and an inland site in Sabah, Malaysian Borneo. *Atmos. Chem. Phys.,* **14,** 8369–8388, doi:10.5194/acp-14-8369-2014.

Rosenberg, P. D., A. R. Dean, P. I. Williams, J. R. Dorsey, A. Minikin, M. A. Pickering, and A. Petzold, 2012: Particle sizing calibration with refractive index correction for light scattering optical particle counters and impacts upon PCASP and CDP data collected during the Fennec campaign. *Atmos. Meas. Tech.,* **5**, 1147–1163, doi:10.5194/amt-5-1147-2012.

Russo, M. R., M. J. Ashfold, N. R. P. Harris, and J. A. Pyle, 2015: On the emissions and transport of bromoform: Sensitivity to model resolution and emission location. *Atmos. Chem. Phys.,* **15,** 14 031–14 040, doi:10.5194/acp-15-14031-2015.

Sherwen, T., and Coauthors, 2016: Iodine's impact on tropospheric oxidants: A global model study in GEOS-Chem. *Atmos. Chem. Phys.,* **16**, 1161–1186, doi:10.5194/acp-16-1161-2016.

Ström, J., R. Busen, M. Quante, B. Guillemet, P. R. A. Brown, and J. Heintzenberg, 1994: Pre-EUCREX intercomparison of airborne humidity measuring instruments. *J. Atmos. Oceanic Technol.,* **11,** 1392–1399, doi:10.1175/1520-0426(1994)011<1392:PEIOAH>2.0.CO;2.

Ulanowski, Z., P. H. Kaye, E. Hirst, R. S. Greenaway, R. J. Cotton, E. Hesse, and C. T. Collier, 2014: Incidence of rough and irregular atmospheric ice particles from Small Ice Detector 3 measurements. *Atmos. Chem. Phys.,* **14,** 1649–1662, doi:10.5194/acp-14-1649-2014.

Whalley, L. K., A. C. Lewis, J. B. McQuaid, R. M. Purvis, J. D. Lee, K. Stemmler, C. Zellweger, and P. Ridgeon, 2004: Two high-speed, portable GC systems designed for the measurement of nonmethane hydrocarbons and PAN: Results from the Jungfraujoch high altitude observatory. *J. Environ. Monit.,* **6,** 234–241, doi:10.1039/b310022g.

Wilson, K. L., and J. W. Birks, 2006: Mechanism and elimination of a water vapor interference in the measurement of ozone by UV absorbance. *Environ. Sci. Technol.,* **40,** 6361–6367, doi:10.1021/es052590c.

Wofsy, S. C., and Coauthors, 2011: HIAPER Pole-to-Pole Observations (HIPPO): Fine-grained, global-scale measurements of climatically important atmospheric gases and aerosols. *Philos. Trans. Roy. Soc.,* **369A,** 2073–2086, doi:10.1098/rsta.2010.0313.